^{17}O NMR study of the doped electrons in lightly oxygen-deficient cubic $SrMnO_{3-x}$

A. Trokiner,[1] S. Verkhovskii,[1,2] Z. Volkova,[2] A. Gerashenko,[1,2] K. Mikhalev,[2] A. Germov,[2] A. Yakubovskii,[3] A. Korolev,[2] B. Dabrowski,[4] and A. Tyutyunnik[5]

[1]*LPEM, ESPCI Paris, PSL Research University, CNRS, Sorbonne Universités, UPMC University, 10 rue Vauquelin, F-75005 Paris, France*

[2]*Institute of Metal Physics, Ural Branch of Russian Academy of Sciences, 620990 Ekaterinburg, Russia*

[3]*Russian Research Centre Kurchatov Institute, 123182 Moscow, Russia*

[4]*Department of Physics, Northern Illinois University, DeKalb, Illinois 60115, USA*

[5]*Institute of Solid State Chemistry, Ural Branch of Russian Academy of Sciences, 620018 Ekaterinburg, Russia*

(Received 2 March 2016; revised manuscript received 27 April 2016; published 18 May 2016)

The spin susceptibility of the localized Mn(t_{2g}) electrons, χ_s, and the spatially distributed spin density of the doped electrons were investigated by ^{17}O nuclear magnetic resonance (NMR) in the paramagnetic (PM) and antiferromagnetic (AF) phases of electron-doped $SrMnO_{3-x}$ ceramics with the cubic structure. Three lightly doped samples ($2x < 0.015$) were studied with $T_N = 220$ K–240 K. In the PM state χ_s increases gradually from T_N and reaches a broad maximum above $\sim 1.5T_N$. The gapped behavior of χ_s indicates a low-dimensional short-range spin order persisting above T_N. These short-range one-dimensional correlations are consistent with ^{17}O NMR results obtained at room temperature, which show that Mn magnetic moments are aligned along the edges of the cubic unit cell. Above 350 K all doped electrons are fast-moving e_g electrons. They provide the uniform polarization of the localized spins which increases χ_s and the increasing doping shifts the oxygen-deficient $SrMnO_{3-x}$ oxide towards a ferromagnetic (FM) metallic state. At lower T the doped electrons are heterogeneously distributed in the oxide: The fraction of the fast-moving electrons diminishes and vanishes below 100 K, while the remaining doped electrons slow down their hopping and each of them creates a FM domain. These FM domains which are detected below 10 K by ^{55}Mn NMR can be considered as small-size magnetic polarons. Their T-activated hopping in the G-type AF lattice was probed by ^{17}O spin-echo experiments. The energy barrier of hopping shows a trend to grow with increasing doping, indicating that the de Gennes metallic ground state cannot be achieved in oxygen-deficient $SrMnO_{3-x}$ oxides, probably due to detrimental oxygen vacancy defects.

DOI: 10.1103/PhysRevB.93.174413

I. INTRODUCTION

The manganese oxides with perovskite structure display a great variety of electronic properties when doped by charge carriers. One of the main issues in the studies of these strongly correlated materials is the ground state emerging from the competition of the antiferromagnetic (AF) superexchange interaction between localized spins and the ferromagnetic (FM) double-exchange (DE) interaction of localized spins with itinerant doped carriers. The magnetic ground state of the lightly doped oxides is considered as nonhomogeneous with FM nanosize domains frozen in the AF lattice when doped with holes [1,2] and with electrons [3–5].

Among the electron-doped manganites, orthorhombic $CaMnO_3$ is one of the most studied compounds. For lightly doped $CaMnO_3$ the existence of FM domains inside the AF lattice was confirmed by both a small-angle elastic neutron scattering [6] investigation of $Ca_{1-x}La_xMnO_3$ ($x = 0.02$) and the ^{17}O nuclear magnetic resonance (NMR) [7] study of $CaMnO_{3-x}$ ($x < 0.01, T_N = 123$ K). According to ^{17}O NMR the Mn spins are almost perfectly aligned in these FM regions. The static and dynamic properties of these domains agree with the model of a small-size self-trapped magnetic polarons (MPs) for which the FM dressing of the trapped electron is mainly stabilized by DE interaction with the core $Mn^{4+}(t_{2g})$ spins [8]. The MP starts to slowly diffuse above 40 K and vanishes in the PM phase at about 30 K above T_N.

Among $SrMnO_3$ polytypes, the cubic perovskite is a rare example of the G-type cubic antiferromagnet. The high symmetry influences several properties, as, for example, the competition of the exchange interactions. Indeed, the increased covalence of the straight Mn-O-Mn bonds enhances the superexchange interaction between the localized Mn(t_{2g}) spins ($T_N \sim 240$ K) [9–12]. In contrast to orthorhombic $CaMnO_3$ with bent Mn-O-Mn bonds, the broad and degenerate e_g-orbital conduction band in $SrMnO_3$ allows a gain in kinetic energy for the doped electrons, placing the *undoped* cubic $SrMnO_3$ close to the borderline between the metallic and insulating states [13–15]. Indeed, cubic $SrMnO_3$ doped by heterovalent substitution of La^{3+} and Ce^{4+} for Sr^{2+} displays a metallic conductivity down to low temperature for electron doping as small as 0.01 per Mn [12], supporting a picture of a canted AF metal as ground state [16]. Investigations with local techniques should confirm this exceptional ground state of electron-doped magnetic oxide.

For a smaller doping level, on the insulating side of the metal-insulator transition, the heterogeneity of the magnetic state in $SrMnO_{3-x}$ ($x \sim 0.001$) is supported by thermally activated conductivity data. This polaronic behavior yields the MP formation energy, $E_a = 25$ meV [4], which is significantly smaller than $E_a \sim 85$ meV in orthorhombic $CaMnO_{3-x}$ ($x < 0.01$) [4,17]. On the other hand, the origin of the FM contribution emerging at low temperature in the reversal isotherms of the bulk magnetization remains controversial [4,11,12]: Is it a phase-separated or a uniform magnetic ground state? In oxygen-deficient $SrMnO_{3-x}$ oxygen vacancies are introduced in the perfectly aligned network of the Mn-O-Mn covalent bonds in order to dope the oxide. Whether further doping of $SrMnO_{3-x}$ renders it more metallic is an open question. Finally, the magnetic transition in $SrMnO_3$ is

generally considered as an order-disorder transition of the local t_{2g} spins, $S = 3/2$, in the isotropic three-dimensional (3D) Heisenberg system but the bulk susceptibility shows no signs of the conventional Curie-Weiss law behavior even far above the transition. This absence indicates the existence of low-dimension short-range magnetic ordering in the paramagnetic (PM) phase far above T_N.

To shed light on these issues we present in this paper the ^{17}O and ^{55}Mn NMR study of lightly electron-doped cubic $SrMnO_{3-x}$ polycrystalline samples ($x < 0.01$). The ^{55}Mn NMR lines of Mn ions in different valence states are generally well separated [18] so that ^{55}Mn NMR is an effective tool to investigate any magnetic heterogeneity existing in the AF lattice (Sec. III B). The thermal behavior of the hyperfine field created at ^{17}O nuclei by the core t_{2g} electrons discloses a gapped behavior of the spin susceptibility in the PM phase (Sec. III C). On the other hand, the thermal behavior of the isotropic component of the hyperfine field shows that among the e_g-doped electrons some are characterized by a fast motion, which provides the uniform polarization of the local t_{2g} spins by means of the de Gennes DE interaction. The low-frequency dynamics of the t_{2g} spins is studied by the ^{17}O spin-echo decay rate, T_2^{-1}, which evidences a slowing down of doped electrons at low temperature (Sec. III D). Finally, we present in Sec. III E T_2^{-1} data which clarify the short-range magnetic correlations of t_{2g} spins in the PM phase of cubic $SrMnO_3$.

II. EXPERIMENTAL DETAILS

Polycrystalline cubic $SrMnO_{3-x}$ ($x < 0.01$) samples were synthesized from a stoichiometric mixture of $SrCO_3$ and MnO_2 by using a two-step method. In the first step, pellets of a single-phase oxygen-deficient perovskite $SrMnO_{2.61}$ were obtained from the precursors fired in flowing argon (containing about 10 ppm O_2 or less) at 1400° C. In the second step, the $SrMnO_{2.61}$ pellet was crushed into powder with an average grain size ~200 mesh. The powder was annealed during 24 h at 550° C in an oxygen gas flow ($P_{O2} \sim 1$ bar) containing ~70% of the ^{17}O isotope, for ^{17}O NMR. The enriched powder was slow cooled to room temperature in the furnace during 26 h. This powder, denoted by S, was then divided into three parts in order to obtain samples with different oxygen deficiencies. The least deficient sample, S1, was obtained by additional annealing of S in an open glass ampoule in a flow of dry air at 230° C during ~2 h. The S2 sample is a part of S with no additional treatment. Finally, the most oxygen-deficient sample, S3, was obtained by annealing a part of S at 280° C during ~3 h in a glass ampoule sealed in air at a pressure of about 0.3 bar.

According to x-ray diffraction all three samples have the cubic ($Pm\bar{3}m$) perovskite structure at room temperature. The lattice parameter, a, grows gradually from S1, S2, to S3 due to the increasing number of vacant oxygen sites. It follows from thermogravimetric study of oxygen-deficient $SrMnO_{3-x}$ ceramics [19] that for $x < 0.01$ the increase of a with x can be approximated with a linear dependence: $a(x) = a(x = 0.0) + 0.425x$, where $a(x = 0.0)$ is the cubic unit cell parameter of the nominally stoichiometric $SrMnO_{3.0}$. The corresponding structural evaluations of x with $a(x = 0.0) = 3.8052$ Å [12] are listed for the S1–S3 samples in Table I.

The bulk magnetization $M(T, H)$ of the samples was measured in the temperature range $T = 2$–330 K with a SQUID magnetometer MPMS-5 (Quantum Design) in magnetic fields $H = 0.01$–5 T and with a vibrating magnetometer PPMS-9 (Quantum Design) up to 9 T. At elevated temperature, 295 K < T < 500 K, dc magnetic susceptibility, $\chi = M/H$ was measured with a Faraday balance technique in $H = 0.15$ T.

The ^{17}O NMR measurements were performed with Bruker NMR spectrometers in the temperature range 7 K–500 K and magnetic fields $H = 1.8$, 9.4, and 11.7 T. Each spectrum was obtained by summing the Fourier-transformed half-echo signals acquired at equidistant operating frequencies. The ^{17}O NMR signal in H_2O was used as a frequency reference $\nu_0 = {}^{17}\gamma H$ for the shift of NMR lines.

In $SrMnO_3$ the resonance frequency of ^{17}O nuclei (spin $^{17}I = 5/2$, quadrupole moment $^{17}Q = -0.025\,78 \times 10^{-24}$ cm^2) is determined by both the magnetic hyperfine interaction and the quadrupolar interaction. The simulation of the spectra obtained at different magnetic fields allows us to determine the magnetic shift components $\{K_i\}$ as well as the quadrupole frequency $\nu_Q = [3e^2Q/2I(2I-1)h]V_{ZZ}$ and asymmetry parameter $\eta = |(V_{XX} - V_{YY})/V_{ZZ}|$ of the electric-field gradient (EFG) tensor $\{V_{ii}\}$. The powder pattern simulation program takes into account the quadrupole coupling corrections up to the second order in $\sim\nu_Q/\nu_0$. Finally, the NMR powder pattern was refined with a Gaussian distribution of the EFG parameters $(\Delta\nu_Q; \Delta\eta)$ and of the isotropic magnetic shifts $(\Delta K_{\rm iso})$.

The ^{55}Mn NMR spectra were obtained in zero magnetic field, $H = 0$, by acquiring the echo signal at equidistant operating frequencies with the two-pulse sequence $(\pi/2) - t - (\pi/2) - t -$ echo. The optimal echo intensity was tuned for each distinct line by changing the amplitude of the pulses, keeping fixed the pulse width $(\pi/2)$ to ~1 μs and the time interval, $t \sim 14$ μs.

The ^{17}O spin-echo decay rate, T_2^{-1}, was measured on the central peak of the ^{17}O NMR spectrum. The echo-decay data were collected using the conventional $\pi/2$-t-π-t-echo pulse sequence. The characteristic time of the echo decay, T_2, is defined as the time at which the echo signal $E(2t)$ drops to $1/e$ of its starting value.

TABLE I. Cubic unit cell parameter at room temperature, a; Néel temperature, T_N; ferromagnetic saturated component, $M_{\rm FM,sat}$, deduced from isotherm magnetization $M(H)$ at $T = 2$ K; oxygen deficiency, x, deduced from x ray.

$SrMnO_{3-x}$ sample	Lattice parameter, a (Å)	T_N (K)	$M_{\rm FM,sat}$(2 K) (μ_B/Mn)	Oxygen deficiency x
S1	3.8061(8)	238.5(30)	0.0151(40)	0.0021
S2	3.8063(8)	238.0(30)	0.0198(40)	0.0026
S3	3.8083(8)	226.0(10)	0.0352(60)	0.0073

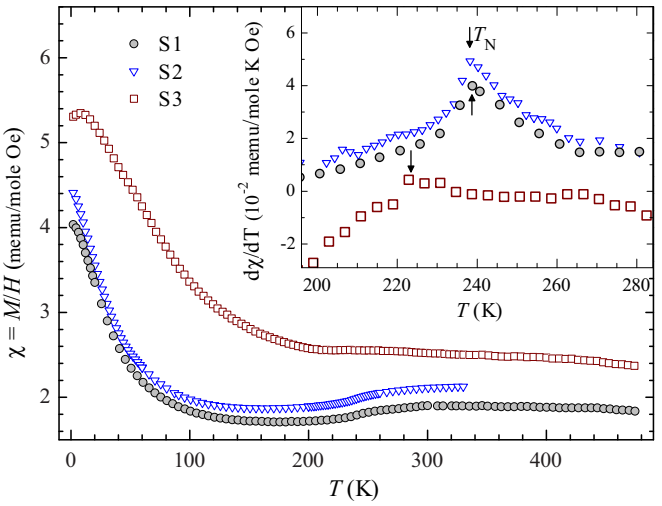

FIG. 1. Temperature dependence of $\chi = M/H$ and $d\chi/dT$ (inset) of $SrMnO_{3-x}$ (S1–S3) samples measured on cooling in $H = 5$ T. The transition temperature T_N is indicated by arrows in the inset.

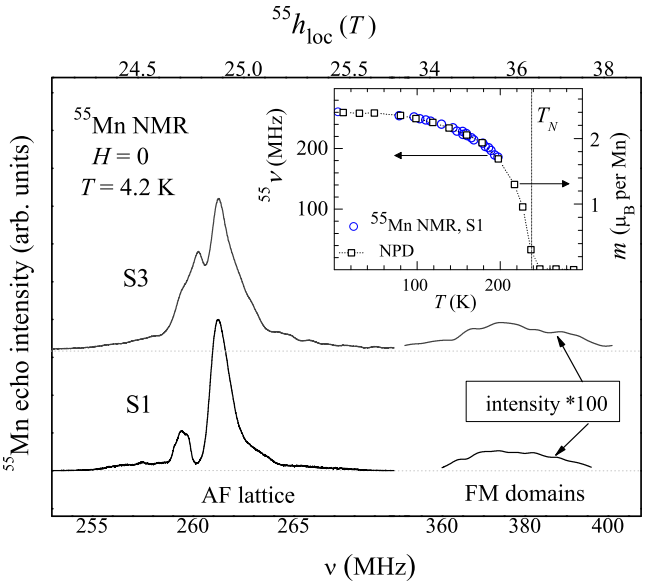

FIG. 2. ^{55}Mn zero-field NMR spectra of the S1 and S3 samples at $T = 4.2$ K. (Inset) Comparison of the thermal dependence of the frequency $^{55}\nu$ of the Mn in AF lattice (S1 sample, $T_N = 238.5$ K) and of the magnetic moment of Mn, m, deduced from neutron powder diffraction study of a nominally stoichiometric $SrMnO_3$ ($T_N = 238$ K) [21].

III. RESULTS AND DISCUSSION

A. Bulk magnetic susceptibility

Figure 1 shows the magnetic susceptibility $\chi = M/H$ of the S1, S2, and S3 samples measured on cooling at $H = 5$ T. For the least-doped S1 and S2 samples, the thermal variation of $\chi(T)$ reproduces the basic features of previous reports for a lightly doped $SrMnO_{2.99}$ [11], a nominally stoichiometric ceramic [10], and a single crystal of $SrMnO_{3.0}$ [12]. These features are (i) a plateaulike behavior in a broad temperature range of the PM state with no signature of the Curie-Weiss law dependence up to ∼500 K, where 500 K is the highest temperature below which x does not vary [9]; (ii) a fairly smooth change of χ when reaching the AF ordered phase (the transition temperature, T_N, was defined as the position of the maximum of $d\chi/dT$ versus T as shown in inset of Fig. 1); (iii) that T_N decreases with increasing x (Table I); (iv) a significant growth of $\chi(T)$ occurs below T_N, with this growth being x dependent. All these features concern the Mn atoms for which the valence and magnetic states can be varied by electron doping.

B. Magnetic heterogeneity at low temperature

1. ^{55}Mn *NMR in the AF phase*

In the magnetic ordered phase, the hyperfine interaction of the ^{55}Mn nucleus (nuclear spin, $^{55}I = 3/2$, and gyromagnetic ratio, $^{55}\gamma = 10.50$ MHz/T) with its nearest electronic environment results in a local field [18]:

$$h_{\mathrm{loc},i} = g_e \mu_B (A S_i + \Sigma_j B_{i,j} S_j). \quad (1)$$

The frequency of ^{55}Mn NMR spectra, $^{55}\nu = (^{55}\gamma/2\pi) h_{\mathrm{loc},i}$, is mainly determined by the "on-site" term, $g_e \mu_B A S_i$, which value is proportional to the number of unpaired $3d$ electrons, S_i, and where $A \sim 10$ T/μ_B is the hyperfine constant [20]. The second term takes into account the effect of the spin density transfer from neighboring magnetic ions S_j. Its contribution to h_{loc} depends on the scalar product $(S_i S_j)$ and is less than 5 T.

Figure 2 shows the ^{55}Mn NMR spectra obtained for the S1 and S3 samples at $T = 4.2$ K in zero field. The spectra consist of two lines. The most intense spectrum is located in a low-frequency range (250–270 MHz), where the NMR signal of the Mn^{4+} is usually detected [18]. With increasing temperature the line adopts a single-peaked shape and its peak position, $^{55}\nu$, is gradually shifted to lower frequency. It is shown in the inset of Fig. 2 for the S1 sample ($T_N = 238.5$ K) that $^{55}\nu(T)$ reproduces well the thermal-averaged magnetic moment, m(Mn), in the sublattices of the AF structure as it was deduced from neutron diffraction data in a nominally stoichiometric $SrMnO_3$ ($T_N = 238$ K) [21].

A significantly less intense line is located at higher frequencies (360–400 MHz) which are typical for ^{55}Mn NMR in FM conducting domains in hole-doped manganites [18]. In these domains the spins of the Mn neighbors are FM aligned due to the DE mechanism and it presumes very fast fluctuating $Mn^{3+} \leftrightarrow Mn^{4+}$ valence state. In addition, the detection of this line shows a significant amplification (∼30) of the radiofrequency magnetic field. This value implies FM domains with negligible magnetic anisotropy.

Thus, ^{55}Mn NMR gives microscopic evidence that at low T in the lightly doped $SrMnO_{3-x}$ samples the FM domains are formed inside the AF ordered lattice of the Mn^{4+} ions. The FM NMR line can be detected only up to about 10 K.

2. *Ferromagnetic component of the bulk magnetization*

The isothermal magnetization curves displayed for the S1 sample on Fig. 3(a) have the same features for all studied samples. Each set of isotherms $M(H)_{T=\mathrm{const}}$ was obtained

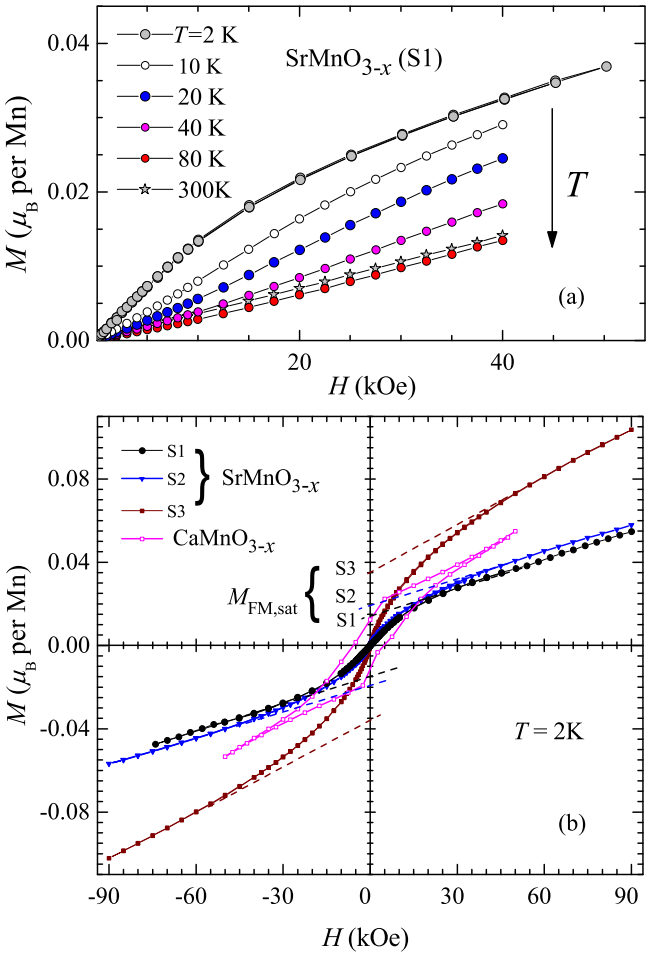

FIG. 3. (a) Isothermal magnetization $M(H)$ of $SrMnO_{3-x}$ (S1) measured after cooling the sample in zero magnetic field. (b) Isothermal magnetization loops $M(H)_{T=2\,K}$ of $SrMnO_{3-x}$ (S1–S3) and $CaMnO_{3-x}$ ($x < 0.01$) [7] at $T = 2$ K.

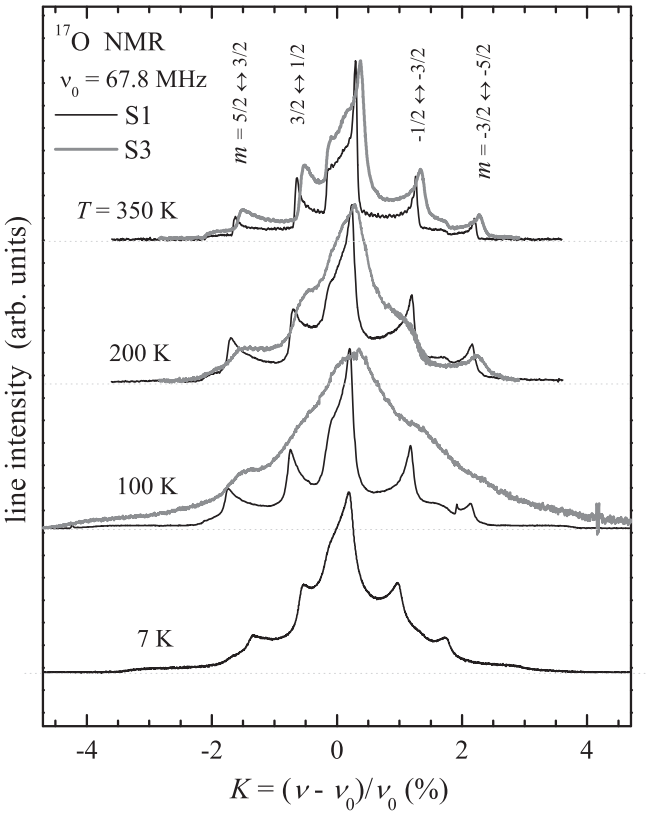

FIG. 4. ^{17}O NMR spectra with all $m \leftrightarrow m-1$ transitions in the paramagnetic and antiferromagnetic phases of the polycrystalline $SrMnO_{3-x}$ (S1 and S3) samples.

by cooling the sample from 300 K down to 2 K in zero magnetic field. Below T_N, $M(H)_{T=\text{const}}$ increases linearly with H. As T decreases down to 40 K, the corresponding slope $(dM/dH)_{T=\text{const}}$ increases gradually mainly due to an additional Curie-like contribution which becomes comparable to that of the canted-in-magnetic-field G-type AF structure, $M_{\text{AF,cant}}$. The nonlinearity of the $M(H)_{T=\text{const}}$ curves appearing below 20 K indicates the emergence of a static FM component, M_{FM}, in the AF phase. The corresponding magnetization reversal curves become a S-shaped (sigmoid shape), as seen in Fig. 3(b). In contrast to the lightly electron-doped $CaMnO_{3-x}$ ($x < 0.01$), there is no hysteresis during the magnetization reversal of $SrMnO_{3-x}$ samples [22]. Using the ^{55}Mn NMR results the magnetization $M(H)$ can be represented as the sum of two contributions,

$$M(H) = M_{\text{AF,cant}} + M_{\text{FM}}, \tag{2}$$

where $M_{\text{AF,cant}}$ increases linearly with H [see the dashed lines in Fig. 3(b)] since the canting angle of the AF ordered Mn magnetic moments is less than 1° in the range of our magnetic fields. M_{FM} is the magnetization of the FM ordered domains. At $H > 3$ T the value of M_{FM} reaches a maximum equal to the saturation magnetization $M_{\text{FM,sat}}$ (Table I).

The $M_{\text{FM,sat}}$ increases regularly in the S1–S3 series, which suggested to us to use $M_{\text{FM,sat}}$ as a measure of the electron doping. For this purpose we assumed that at low T the $2x$-doped electrons are well separated from each other in space and each doped electron was captured inside the isolated FM domain, forming a MP with an effective magnetic moment, $m_{\text{MP}} = M_{\text{FM,sat}}(2\text{ K})/2x$. With this definition, $x = 0$ for $M_{\text{FM,sat}} = 0$ represents a truly stoichiometric $SrMnO_{3.00}$ compound.

C. ^{17}O NMR shift and local spin susceptibility

Some representative ^{17}O NMR spectra acquired in the PM and AF phases of the $SrMnO_{3-x}$ samples are shown on Fig. 4.

In the PM phase the features of the powder spectrum are well described with a single set of parameters of the EFG tensor ($\nu_Q = 1.06$ MHz; $\eta = 0$) and the magnetic shift tensor ($K_{\text{iso}}, K_{\text{ax}}$). The axial symmetry of both tensors is in accordance with the $D4h$ local symmetry of the O site. In particular, one can write, $K(\alpha) = K_{\text{iso}} + K_{\text{ax}}(3\cos 2\alpha - 1)$, where α is the angle between H and the Mn-O-Mn bonds direction and $K(\alpha)$ is the ^{17}O magnetic shift for this orientation. Figure 5 shows the T dependence of the isotropic, K_{iso}, and axial, K_{ax}, components of the ^{17}O magnetic shift in the three samples. When T decreases, K_{iso} and $|^{17}K_{\text{ax}}|$ decrease and they increase when the doping increases.

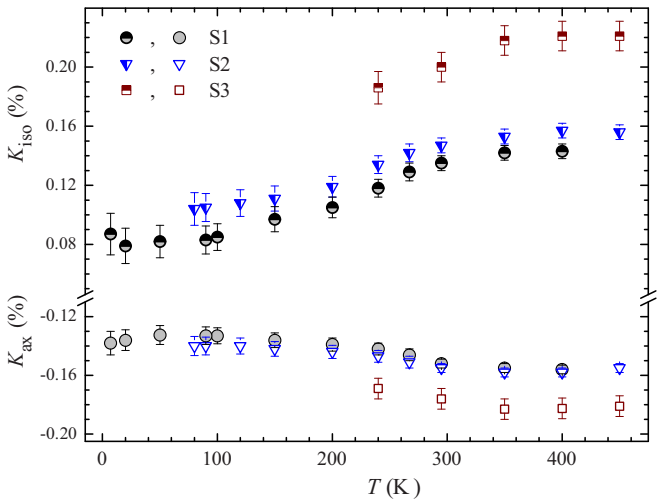

FIG. 5. Temperature dependence of the isotropic, $^{17}K_{iso}$, and axial, $^{17}K_{ax}$, components of the ^{17}O NMR magnetic line shift in cubic $SrMnO_{3-x}$.

Let us consider the temperature dependence of K_{ax} in the PM phase. As K_{ax} relates to the axial component of the shift tensor it is due to the axial component, h_{ax}, of the local field, which has two contributions, h_{dip} and h_{hf}. The former originates from the dipole-dipole interaction between the ^{17}O nuclear magnetic moment and the localized magnetic moments of its Mn^{4+} neighbors, while h_{hf} is due to the anisotropic part of the hyperfine interaction [23]:

$$K_{ax}(T,x)H = h_{ax} = h_{dip,ax} + h_{hf,ax}. \quad (3)$$

The classic dipole field h_{dip} was calculated by using the structural data $r_{Mn\text{-}O}$ (Table I and Ref. [21]) and the magnetic moment $m_{z\|H}(Mn) = \chi_{mol}(T)H/N_A$. Almost T-independent values have been obtained for the axial component, $K_{dip,ax}(S1) = 0.10(1)\%$, $K_{dip,ax}(S2) = 0.11(1)\%$, and $K_{dip,ax}(S3) = 0.13(1)\%$; the thermal changes in the PM phase are denoted in parentheses. As the difference $K_{ax}(T) - K_{dip,ax}$ defines the axial component of the hyperfine shift $K_{hf,ax}(T)$, the temperature variation of $K_{hf,ax}(T)$ is traced by the $K_{ax}(T)$ raw data (Fig. 5). Because of the sizable covalence of the Mn(d)-O($2p$) bond, spin densities are transferred from Mn orbital to O orbital [24,25], producing the hyperfine field, $h_{hf,ax} = K_{hf,ax}H$. Indeed, a spin density, $s_z(2p_\pi) = f_\pi S_z(t_{2g})$, is transferred on the O-$2p_\pi$ orbitals from two single-occupied Mn-t_{2g} orbitals so that

$$h_{hf,ax}(2p_\pi) = -4/5\mu_B\langle r^{-3}\rangle_{2p} f_\pi \langle S_z(t_{2g})\rangle, \quad (4)$$

where f_π is the fractional occupancy of the O-$2p_\pi$ orbital by an unpaired Mn spin and the thermal average $\langle S_z(t_{2g})\rangle$ is related to χ_s, the local spin susceptibility of the localized $S(t_{2g})$ spin of $Mn^{4+}(^3t_{2g}{}^0e_g)$ ions, by the relation $\chi_s = g\mu_B\langle S_z(t_{2g})\rangle/H$. Another spin density, $s_z(2p_\sigma)$, is created at the O-$2p_\sigma$ orbital by the delocalized doped electrons participating to the fast hopping between Mn sites. We define $n_{e_g}/2x$ as the fraction of these delocalized doped electrons, and because $2x$, the total number of doped electron per Mn, is small (see Table I), $n_{e_g} \ll 1$. These electrons become itinerant in the conduction O($2s2p_\sigma$) − Mn(e_g) band, having dominant e_g character with the density of states $g(E)$ [13,14]. Because of the strong intra-atomic exchange interaction with the almost localized t_{2g} electrons, $-J_s(e_g)S(t_{2g})$, the band consists of spin-up polarized states and an unpaired spin $s_z(e_g) = g(E_F)JS_z(t_{2g})$ [23] appears at the Mn-e_g orbital in doped $SrMnO_{3-x}$. The spin density transferred at the O-$2p_\sigma$ orbital from the itinerant e_g electrons can be expressed in terms of the partial density of states $g_\sigma(E_F) = f_\sigma g(E_F)$: $s_z(2p_\sigma) = f_\sigma g(E_F)JS_z(t_{2g})$. The corresponding contribution $h_{hf,ax}(2p_\sigma)$ to $h_{hf,ax}$ is

$$h_{hf,ax}(2p_\sigma) = 4/5\mu_B\langle r^{-3}\rangle_{2p} f_\sigma g(E_F)J\langle S_z(t_{2g})\rangle. \quad (5)$$

At very small levels these n_{e_g}-doped electrons do not interact with each other and are in the lowest energy state at the bottom ($q = 0$) of the e_g band [26]. Furthermore, the density of electronic states increases proportionally to the filling, $g(E_F) \sim n_{e_g}/E_F$. Finally, the anisotropic component of the hyperfine field results in

$$K_{hf,ax} = h_{hf,ax}/H = -4/5\mu_B\langle r^{-3}\rangle_{2p}\langle S_z(t_{2g})\rangle \times\left(f_\pi - n_{e_g} f_\sigma J/E_F\right)/H. \quad (6)$$

As $n_{e_g} f_\sigma J/E_F$ is negligible compared to f_π [27], the thermal behavior of $|K_{hf,ax}|$ is the one of $\chi_s(T)$. The negative slope of $K_{hf,ax}$ yields a positive slope for $d\chi_s/dT$ and thus a gapped behavior of $\chi_s(T)$ for all the samples. The gapped behavior of the local spin susceptibility is almost masked in the bulk magnetization data of this work, as well as in previously published results in cubic $SrMnO_3$ [4,10–12]. It is worth to notice that this behavior is in contrast with the classic mean-field behavior, $\chi_s \sim (T - \theta)^{-1}$, observed in $CaMnO_3$ above the 3D magnetic order-disorder transition [17,28]. These different $\chi_s(T)$ behaviors can be related to the competition of Mn(t_{2g}) − O($2p_\pi$) − Mn(t_{2g}) and Mn(t_{2g}) − O($2p_\pi$) − Sr/Ca − O($2p_\pi$) − Mn(t_{2g}) superexchange interactions between the nearest and the next-nearest Mn^{4+} ions, respectively [29,30]. In *cubic* $SrMnO_3$ this competition is geometrically frustrated due to the t_{2g} orbital degeneracy; such frustration should favor short-range correlations between Mn spins. The breakdown of the Curie-Weiss law for $\chi_s(T)$ may indicate the persistence of short-range spin correlations between neighboring magnetic Mn^{4+} ions far above T_N.

The isotropic shift has two contributions in the PM phase of $SrMnO_{3-x}$, similar to $CaMnO_{3-x}$ [17],

$$K_{iso}(T,x) = K_0 + K_{hf,iso}(T,x), \quad (7a)$$

where the chemical shift, $K_0 = K_{iso}(T = 20\text{K}) = 0.08\%$, is independent of T and x and the T-dependent spin contribution is the hyperfine isotropic shift $K_{hf,iso}(T,x) = h_{loc}(2s)/H$. In the doped samples the local field $h_{loc}(2s)$ is due to the Fermi contact interaction of the nuclear spin ^{17}I with the s-spin density $s_z(2s)$ of the delocalized electrons [31] $\langle s_z(2s)\rangle = f_s n_{e_g} J/E_F\langle S_z(t_{2g})\rangle$ and

$$K_{hf,iso}(T) = h_{loc}(2s)/H = 2H_{FC}(2s)f_s\langle s_z(e_g)\rangle/H = 2H_{FC}(2s)f_s(J/E_F)n_{e_g}\langle S_z(t_{2g})\rangle/H. \quad (7b)$$

Here the hyperfine magnetic field $H_{FC}(2s)$ is created by one unpaired electron residing at the O($2s$) orbital. According to Eqs. (6) and (7b) the ratio $K_{hf,iso}(T)/|K_{hf,ax}|$ is proportional to

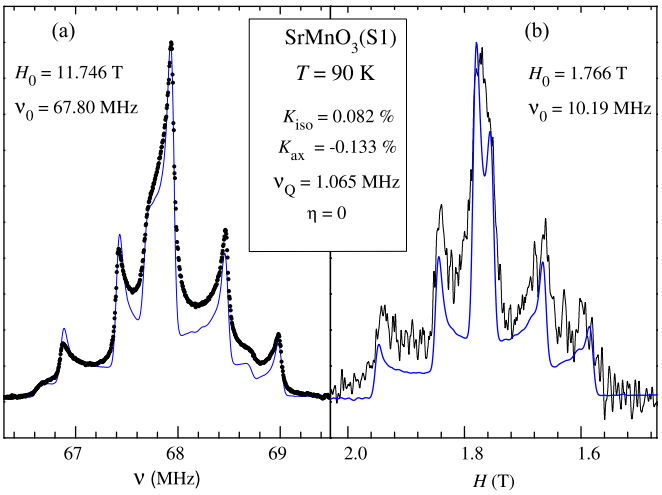

FIG. 6. ^{17}O NMR spectra obtained for $SrMnO_{3-x}$ (S1) sample in two magnetic fields 11.76 T (a) and 1.7 T (b). The blue curves show the best fit obtained with the same set of magnetic shift (K_{iso}, K_{ax}) and EFG (ν_Q, η) parameters for both spectra.

n_{e_g}, the number of the fast-moving e_g electrons per Mn. These electrons enhance the uniform polarization of the localized $S_z(t_{2g})$ spins in the doped $SrMnO_{3-x}$ through the de Gennes double-exchange mechanism [16]. Moreover, both $K_{hf,iso}$ and $|K_{hf,ax}|$ reach a broad maximum above 350 K, indicating that at higher temperatures the doped electrons are all fast-moving e_g electrons, $n_{e_g} = 2x$. Since $|K_{hf,ax}|$ traces the thermal variation of χ_s, the increase with doping of the maximum of χ_s is evidence that at elevated temperatures in the PM phase the cubic oxygen-deficient $SrMnO_{3-x}$ oxide shifts towards the FM metallic state by electron doping.

Below T_N, the Mn moments are ordered in two magnetic sublattices—$\boldsymbol{M}_1 = \boldsymbol{m}_1 N_A/2$, $\boldsymbol{M}_2 = \boldsymbol{m}_2 N_A/2$—with the staggered moment $\boldsymbol{M}_{stagg} = \boldsymbol{M}_1 - \boldsymbol{M}_2$. At $H = 0$ the G-type AF ordering preserves the inversion symmetry $(\boldsymbol{r} \leftrightarrow -\boldsymbol{r})$ of the O sites (positions 6*b*) [32]. As a result, the hyperfine and dipole local fields vanish at the O site because they are due to both magnetic moments, $\boldsymbol{m}_1$ and $\boldsymbol{m}_2 = -\boldsymbol{m}_1$. In an external magnetic field the inversion symmetry of the O site is broken due to the canting of the AF structure and the local fields which define the ^{17}O NMR shift components are now controlled by $\boldsymbol{M}_{AF,cant} = \boldsymbol{M}_1 + \boldsymbol{M}_2 = \boldsymbol{m}_{FM} N_A$, where $\boldsymbol{m}_{FM}$ is the FM moment per Mn of the canted AF structure.

In each AF domain of the powder sample the $\boldsymbol{m}_{FM}$ is directed along the effective field $\boldsymbol{H}_{eff} = \boldsymbol{H} + \boldsymbol{H}_a$, where the magnetic anisotropy field, $\boldsymbol{H}_a$, is an intrinsic feature of the crystallites [33]. Even in a structurally perfect powder the misalignment of $\boldsymbol{m}_{FM}$ causes a field-dependent magnetic broadening of the spectrum $\Delta K = (\Delta H)/H \sim H_a/(H + H_a)$. However, upon cooling the sample in a very large magnetic field, $H \gg H_a$, one obtains below T_N a magnetically oriented powder; i.e., in each grain $\boldsymbol{m}_{FM}$ is parallel to $\boldsymbol{H}$ whatever the orientation of the grain in the magnetic field. This situation can be considered similar to the one in the PM phase where the magnetization, $\boldsymbol{m}_z = g\mu_B H \langle Sz(t_{2g})\rangle$ is the z projection on the $\boldsymbol{H}$ direction.

The ^{17}O NMR spectra in Figs. 4 and 6 were acquired after cooling the powder samples from room temperature down to $T < T_N$. In the AF phase, the spectra of the most structurally ordered samples (S1 and S2) preserve the quadrupolar split structure showing only a minor magnetic broadening of the peaks, $(\Delta H) \sim 0.02$ T. Because (ΔH) varies only slightly with H the magnetic anisotropy field can be evaluated as $H_a \leqslant 0.02$ T [34] and the condition $H_a \ll H$ is fulfilled for all ^{17}O NMR spectra discussed in this work. Our samples being tightly packed powders, the grains are still randomly oriented below T_N, as in the PM state, with $\boldsymbol{m}_{FM} \parallel \boldsymbol{H}$ in each grain. Thus, it is still meaningful to simulate the NMR spectra in the AF phase by considering an assembly of randomly oriented grains. As Fig. 6 shows, the $T = 90$ K ^{17}O NMR spectra obtained at 1.8 and 12 T are well described by the curves calculated for the powder pattern simulation program with the same EFG parameters (ν_Q, η) and, more importantly, with the same magnetic shifts (K_{iso}, K_{ax}). The excellent fit at both, 1.8 and 12 T, shows that the deduced shift parameters, K_{iso} and K_{ax}, do not depend on H. This is unusual in a magnetic ordered phase. This H independence confirms that the local fields are proportional to H, such that in the AF phase we may trace the thermal variation of the ^{17}O local fields by using the spectral data of $K_{iso}(T)$ and $K_{ax}(T)$ (Fig. 5). Moreover, the data can be compared to Eqs. (6) and (7b), where the thermal average $\langle S_z(t_{2g})\rangle$ is replaced with $m_{FM}/g\mu_B$. Moreover, according to neutron diffraction data [10,35] and to our ^{55}Mn NMR data, the AF structure is completely formed at $T = 80$ K with magnetic moment per Mn of $m_1 = m_2 \sim 2.5\mu_B$ [10]. The hyperfine component $|K_{hf,ax}| = |K_{ax} - K_{dip,x}|$ which is proportional to $m_{FM}(T)$ is T independent below 80 K, confirming that the in-field-canted AF structure remains invariable at lower T. Finally, the fact that the local fields at the O site are proportional to H demonstrates that the canted magnetic structure appears *only* in an external magnetic field.

The thermal behavior of $K_{hf,iso}$, $|K_{hf,ax}|$ and the bulk magnetization, $\chi(T)$, above and below T_N are compared in Fig. 7(a). The values of $|K_{hf,ax}|$ and $K_{hf,iso}$ were deduced, respectively, from Eqs. (3) and (7a), with $K_0 = 0.08\%$ and rescaled in χ units so that both parameters match χ at $T = 400$ K. The thermal behaviors are different for all three quantities.

The T dependence of $|K_{hf,ax}|$ and $\chi(T)$ are very similar down to $T \sim 150$ K in the AF phase, where $\chi(T)$ start to deviate from the gapped behavior. Since $|K_{hf,ax}|$ varies as the FM moment of the canted AF structure, m_{FM}, the strong growth of $\chi(T)$ indicates the existence of a contribution which adds to the AF contribution; it is presumably due to FM domains which were observed by the ^{55}Mn NMR (Fig. 2) [36]. In contrast, $K_{hf,iso}$ deviates from $|K_{hf,ax}|$ and $\chi(T)$ already in the PM phase, below $T \sim 350$ K. The different T dependencies of $|K_{hf,ax}|$ and $K_{hf,iso}$ are in agreement with Eqs. (6) and (7b), respectively, where $|K_{hf,ax}(T)|$ varies proportionally to $\langle S_z(t_{2g})\rangle$, whereas $K_{hf,iso}(T)$ is proportional to $n_{e_g}\langle S_z(t_{2g})\rangle$. As shown in Fig. 7(b), n_{e_g} starts to decreases in the PM phase and continues to decrease in the AF phase with no influence of the PM-AF phase transition on its thermal behavior. Thus, for all samples, as T diminishes below $T \sim 350$ K, an increasing fraction of fast-moving doped electrons slow down their motion. These $(2x - n_{e_g})$ electrons are not detected in the NMR windows shown in Figs. 4 and 6. They are presumably located inside the

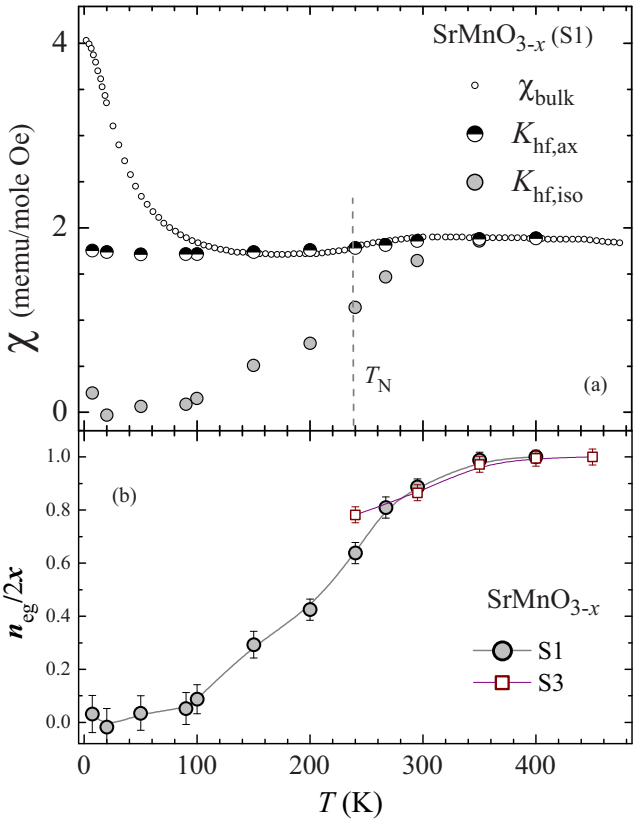

FIG. 7. (a) Comparison of the thermal behavior of $\chi = M/H, K_{\mathrm{hf,iso}}$ and $|K_{\mathrm{hf,ax}}|$ in $SrMnO_{3-x}$ sample S1. The values of $K_{\mathrm{hf,iso}}, |K_{\mathrm{hf,ax}}|$ have been multiplied by normalizing factors so that at $T = 400$ K they match the χ value. (b) Fraction of fast hopping electrons $n_{e_g}/2x = \{K_{\mathrm{hf,iso}}(T)/|K_{\mathrm{hf,ax}}(T)|\}/\{K_{\mathrm{hf,iso}}(400\,\mathrm{K})/|K_{\mathrm{hf,ax}}(400\,\mathrm{K})|\}$ vs T in $SrMnO_{3-x}$ samples (○, S1; □, S3).

FM domains. This conjecture is supported by the conductivity measurements published for a lightly doped $SrMnO_{3-x}$ [4], where the observed activated behavior can be interpreted as due to the motion of small-size magnetic polarons. Such nanosize magnetic heterogeneity is the most probable source of the substantial growth of χ at low T (Fig. 1).

D. Dynamics of the magnetic polarons

In the AF lattice the random walk of a MP is accompanied by temporal perturbations of the ground configuration ($\uparrow\downarrow$) of the neighboring Mn moments, yielding a time-dependent local field at ^{17}O nuclei. Indeed, when an oxygen nucleus is captured during the time τ_1 inside a FM polarized MP region, its resonance frequency, $^{17}\nu$, is shifted from $\nu_{\mathrm{AF}} = \gamma h_{\mathrm{AF}}$ (NMR window in Fig. 4) to a higher frequency, $\nu_{\mathrm{FM}} = \gamma h_{\mathrm{FM}}$. When the MP moves away, the oxygen nuclei is again in the AF lattice and $^{17}\nu$ returns to ν_{AF}, keeping this value during τ_0 until the oxygen atom is again trapped by MPs. As at small concentration of doped electrons $\tau_1 \ll \tau_0$, the walking MPs induce a "pulselike" fluctuating local field at ^{17}O nuclei. As T decreases, the MP diffusion slows down and both characteristic duration τ_1 and τ_0 increase. Their values can be probed in ^{17}O spin-echo experiments.

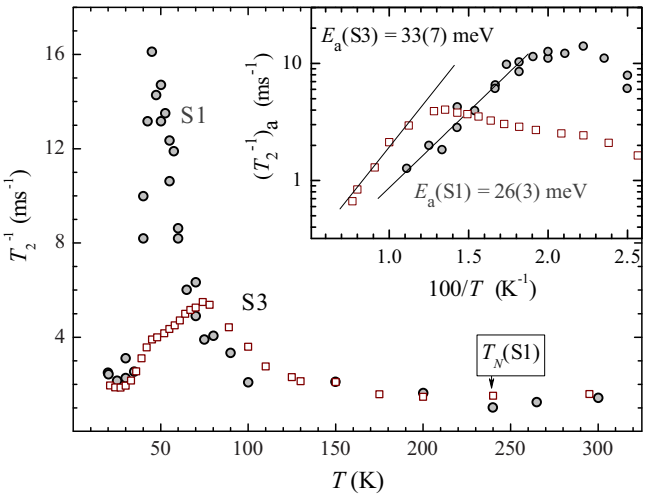

FIG. 8. Rate of ^{17}O echo decay, T_2^{-1} vs T in $SrMnO_{3-x}$ (S1 and S3). (Inset) Arrhenius plot of $(T_2^{-1})_a = T_2^{-1}(T) - T_2^{-1}(200\,\mathrm{K})$ vs $100/T$, the solid lines are a linear fit of the (T_2^{-1}) data above 50 K.

The decay rate of the spin-echo signal was measured on the central peak of the ^{17}O NMR spectra at $H = 11.7$ T to be much larger than the local fields h_{AF} and h_{FM}. Figure 8 shows the T_2^{-1} raw data collected in the PM and AF phases of the S1 and S3 samples. In both samples T_2^{-1} is almost constant from 300 K down to $\sim T_N/2$. Then a peaked behavior is observed when the Mn moments stop to vary (inset of Fig. 2) since the AF structure is completely formed [21]. On the high-temperature side of the peak the difference $(T_2^{-1})_a = [T_2^{-1}(T) - T_2^{-1}(200\,\mathrm{K})]$ increases following the Arrhenius law $(T_2^{-1})_a \sim \exp(E_a/T)$ with an energy barrier $E_a(\mathrm{S1}) = 26(2)$ meV and $E_a(\mathrm{S3}) = 33(7)$ meV.

In a polaronic scenario E_a can be associated to the MP formation, i.e., the energy which is released when the doped electron slows down its motion and creates a FM alignment of its surrounding Mn spins. The value of the energy barrier $E_a(\mathrm{S1}) = 26$ meV is in agreement with $E_a = 25$ meV [4] obtained from electrical conductivity data in a polycrystalline cubic $SrMnO_3$ ($n_e \sim 10^{-3}$ per Mn). Moreover, the MP formation energy $E_a(\mathrm{S1})$ is three times less than $E_a = 86$ meV obtained by ^{17}O NMR in orthorhombic $CaMnO_{3-x}$ [17]. The significantly reduced formation energy in $SrMnO_{3-x}$ is consistent with the rather large fraction $n_{e_g}/2x$ of fast-moving doped electrons still existing in the AF lattice [Fig. 7(b)]. Nevertheless, with increasing x the E_a barrier shows a trend to grow, indicating that the de Gennes metallic ground state cannot be achieved in oxygen-deficient $SrMnO_{3-x}$. In contrast, a metallic conductivity was evidenced in heterovalent $(Sr^{2+} - La^{3+}; Ce^{4+})$ doped $SrMnO_3$ [12].

It should be noted that these ^{17}O NMR data probe the local hopping of electrons near oxygen atoms while the conductivity data yield the average-over-crystal parameters of the diffusive electron motion. The closeness of both E_a estimates implies a Brownian motion of the doped electrons with no local back-and-forth jumps.

The T_2^{-1} value is determined by the time fluctuating field $\boldsymbol{h} = \{h_\perp, h_\parallel\}$. With magnetization measurements [Fig. 3(b)] and with ^{17}O NMR in the AF phase, it is reasonable to consider

that at high field the longitudinal component, $h_\parallel$, is defined by the direction of H with $h_\parallel = h_{\rm FM} - h_{\rm AF}$. In general, both $h_\perp$ and $h_\parallel$ contribute to the echo-decay process [37–39],

$$T_2^{-1}(T) = \{(\gamma h_\parallel \tau_1)^2/\tau_0[1 + (\gamma h_\parallel \tau_1)^2]\} + ({}^{17}I + 1/2)^2 T_1^{-1}(T), \quad (8)$$

where the nuclear spin-lattice relaxation rate, T_1^{-1}, involves only the transverse component, $h_\perp$, probing $h_\perp(t)$. The T_1^{-1} data obtained below T_N yield the inequality $T_1^{-1} < 0.01 T_2^{-1}$, which makes it possible to take into account only the first term in Eq. (8). Hereinafter, the peaked behavior of $(T_2^{-1})_a$ is analyzed in terms of τ_1 and τ_0, the time durations characterizing the MP motion. Below 100 K almost all doped electrons have slowed down [Fig. 7(b)] so that the ratio τ_1/τ_0 is no more T dependent. It is worth underlining that T_2^{-1} is measured on the oxygen nuclei belonging to the AF matrix. During the measurement, when an oxygen nucleus is captured by a MP during τ_1, its frequency is changed, yielding a dephasing so that its signal does not contribute anymore to the refocusing of the spin echo. The corresponding dephasing angle is $\gamma h_{\rm FM} \tau_1$. Assuming that on the high-T side of the $(T_2^{-1})_a$ peak the dephasing angle is small, $\gamma h_{\rm FM} \tau_1 \ll 1$, the form of Eq. (8) can be simplified as

$$\left(T_2^{-1}\right)_a = (\gamma h_\parallel \tau_1/\tau_0)^2 \tau_0(T), \quad (8a)$$

showing the proportionality of $(T_2^{-1})_a \sim \tau_0(T) \sim \exp(E_a/T)$. Whereas on low-$T$ side of the peak, the slow-motion regime with $\gamma h_{\rm FM} \tau_1 \gg 1$ can be considered:

$$\left(T_2^{-1}\right)_a = 1/\tau_0(T). \quad (8b)$$

Now the $(T_2)_a$ value is a direct estimate of τ_0, the time during which the oxygen atom is in the AF ordered lattice between two subsequent captures by MPs. The maximum of $(T_2^{-1})_a$ occurs when $\gamma h_{\rm FM} \tau_1 = 1$. By taking ${}^{17}\gamma\, h_\parallel \sim 1.5 \times 10^8$ s^{-1} [7], one obtains an estimate of $\tau_1(50\ {\rm K}) \sim 6.4 \times 10^{-9}$ s and $\tau_0(50\ {\rm K}) \sim 3.5 \times 10^{-5}$ s for the S1 sample. For the S3 sample, the shift of $(T_2^{-1})_a$ peak toward higher temperature ~80 K indicates a slower MP motion. Indeed, one may evaluate that τ_1 (80 K, S3 sample) ~τ_1 (50 K, S1 sample). Thus, as the doping increases, the growth of the energy barrier yields a slowdown of the MP motion.

E. Anisotropy of the Mn spin fluctuations in the paramagnetic phase

In the PM phase the magnitude and direction of the time-dependent components, $\{h_\perp; h_\parallel\}$, of the local field are still determined by the fluctuations of the electron spin of the neighboring Mn. Away from T_N the exchange-coupled electron spins fluctuate with a frequency $\omega_{\rm ex} = 2\pi/\tau_c$ much larger than ω_0, the ^{17}O NMR frequency yielding $\omega_0 \tau_c \ll 1$. This inequality makes it possible to use simplified expressions of T_1^{-1} and T_2^{-1} [39,40]:

$$T_1^{-1} = \gamma^2 \langle h_\perp^2 \rangle \tau_c, \quad (9a)$$

$$T_2^{-1} = \gamma^2 [\langle h_\parallel^2 \rangle + ({}^{17}I + 1/2)^2 \langle h_\perp^2 \rangle] \tau_c. \quad (9b)$$

The echo decay measurements disclosed a dependence of T_2 on α, the angle between $\boldsymbol{H}$ and the cubic axes. In the S1 sample we measured $1.11(9)\ {\rm ms}^{-1} \leqslant T_2^{-1}(300\ {\rm K}) \leqslant 1.44(9)\ {\rm ms}^{-1}$. Following Eqs. (9) we define the ratio $R \equiv \{[T_2^{-1}/T_1^{-1}] - 9\} = \langle h_\parallel^2 \rangle / \langle h_\perp^2 \rangle$, where $\langle h_\parallel^2 \rangle$ and $\langle h_\perp^2 \rangle$ are the mean square of the fluctuating components along and perpendicular to $\boldsymbol{H}$, respectively. The parameter R measures the anisotropy of the fluctuating local field. In the S1 sample we measured $T_1^{-1}(300\ {\rm K}) = 0.052(5)\ {\rm ms}^{-1}$, yielding $12.4 < R < 18.7$. These values exceed considerably the $R = 0.5$ deduced in $CaMnO_3$ for which the spin fluctuations are isotropic [41].

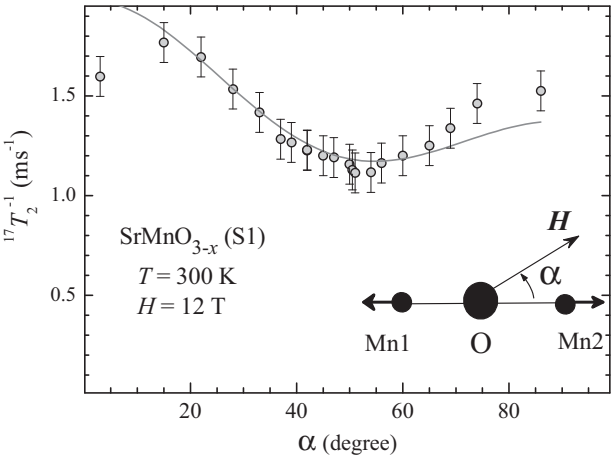

FIG. 9. The rate of ^{17}O echo decay, $^{17}T_2^{-1}$, versus the angle α (see text and insert) for $SrMnO_{3-x}$ (S1) at $T = 300$ K.

Figure 9 shows the T_2^{-1} dependence on α. The solid curve is a fit with the expression $A + B(\alpha)$, where the α-dependent part is

$$T_2^{-1}(\alpha) = \left(T_2^{-1}\right)_0 \tfrac{1}{4}(3\cos^2\alpha - 1)^2, \quad (10)$$

where $(T_2^{-1})_0$ is proportional to the square of the local field for $\alpha = 0$, i.e., when the magnetic moments are parallel to the Mn-O-Mn bond.

The fitting curve reproduces the features of the $T_2^{-1}(\alpha)$ dataset in a wide range of angles. $T_2^{-1}(\alpha)$ shows a maximum for $\alpha = 0$, i.e., for Mn magnetic moments parallel to the Mn-O-Mn bond and a minimum for the "magic" angle value $\alpha_{\rm magic} = \arccos(1/3)^{1/2}$ for which the contribution of the dipole field vanishes. The two datasets $T_2^{-1}(\alpha)$ collected at 7 and 2 T (not shown) display also a maximum at $\alpha \sim 0$ and a minimum for $50^\circ < \alpha < 60^\circ$. It is worth noting that both $h_{\rm hf,nn}$ and $h_{\rm dip,nn}$, created by the Mn nearest neighbors, have the same α dependence with a maximum for $\alpha = 0$ and zero value for $\alpha_{\rm magic}$. Moreover, the α dependence of T_2^{-1} is mainly monitored by $[h_{\rm hf,nn}(\alpha)]^2 \sim (3\cos 2\alpha - 1)^2$ since, on one hand, $|h_{\rm hf,nn}|$ is about three times larger than $|h_{\rm dip,nn}|$ and, on the other hand, the dipolar fields of more distant Mn moments have only minor effect on the $T_2^{-1}(\alpha)$ dependence. Thus, the main fluctuations correspond to *Mn magnetic moments aligned along the edges of the cubic unit cell*, evidencing a 1D short-range correlated ordering in PM phase, in agreement with the abnormally large value of $R = \langle h_\parallel^2 \rangle / \langle h_\perp^2 \rangle$.

The most likely origin of this 1D short-range magnetic order is connected to the fluctuations of the exchange-coupled spin pair of Mn first neighbors, e.g., Mn1 and Mn2, shown

in the inset of Fig. 9, in which the instant configuration of S1 and S2 spins is not only the ground singlet ($\boldsymbol{S}_1 + \boldsymbol{S}_2 = 0$) state but also the excited triplet ($\boldsymbol{S}_1 + \boldsymbol{S}_2 = 2\boldsymbol{S}$). In this case, the longitudinal component, $h_\parallel$, changes randomly between $h_{\text{singlet}} \sim 0$, corresponding to ($\boldsymbol{S}_1 + \boldsymbol{S}_2 = 0$) and $h_{\text{triplet}} \gg h_{\text{singlet}}$, corresponding to ($\boldsymbol{S}_1 + \boldsymbol{S}_2 = 2\boldsymbol{S}$). The ^{17}O resonance frequency is $\nu_{\text{singlet}} = \gamma h_{\text{singlet}} \sim 0$ during the time τ_{singlet} and $\nu_{\text{triplet}} = \gamma h_{\text{triplet}} \sim 25$ MHz during the time τ_{triplet} [7]. The ratio $\tau_{\text{triplet}}/\tau_{\text{singlet}}$ is equal to the ratio of the probabilities to find the Mn neighbors in the triplet or singlet configurations, $P_{\text{triplet}}/P_{\text{singlet}}$. For the S1 sample with $T_N = 238.5$ K the characteristic frequency of Mn spin fluctuations of the exchange coupled pair in the ground singlet state, $\omega_{\text{ex}} \sim 5 \times 10^{12}\text{s}^{-1}$ [42] yields $\tau_{\text{singlet}} = 2\pi/\omega_{\text{ex}} \sim 1.1 \times 10^{-12}$ s.

As a short-range magnetic order exists between Mn nearest neighbors, it is reasonable to consider that $\tau_{\text{triplet}}/\tau_{\text{singlet}} \ll 1$. For such a pulselike varying local field we may use Eq. (8a) in order to express $(T_2^{-1})_0$ introduced in Eq. (10):

$$\left(T_2^{-1}\right)_0 = (\gamma h_\parallel P_{\text{triplet}}/P_{\text{singlet}})^2 2\pi/\omega_{\text{ex}}. \tag{11}$$

As $\omega_{\text{ex}} \sim 5 \times 10^{12}$ s^{-1}, we find at room temperature $P_{\text{triplet}}/P_{\text{singlet}} \sim 0.15$ and thus obtain a quantitative description of the correlated anisotropic (1D) spin fluctuations of the Mn neighbors which exist in the PM phase of *cubic* $SrMnO_3$.

IV. CONCLUSION

The cubic, lightly charge-doped $SrMnO_{3-x}$ perovskite was investigated by ^{17}O NMR. Three polycrystalline samples with different electron doping levels ($2x < 0.015$) were studied in the PM and AF G-type phases ($T_N = 220$ K–240 K). Measurements of the hyperfine fields created at the oxygen nuclei by the surrounding electrons make it possible to clarify the intrinsic thermal behavior of the localized Mn(t_{2g}) spins and the spatially distributed spin density of the doped electrons.

In the PM state the spin susceptibility of the t_{2g} electrons, $\chi_s(t_{2g})$, increases gradually from T_N, reaching a broad maximum above $\sim 1.5T_N$ with no indication of mean-field behavior, i.e., the Curie-Weiss law. Instead, $d\chi_s/dT \geqslant 0$ is evidence of a gapped behavior indicative of a low-dimensional short-range spin order persisting far above the 3D magnetic transition. Furthermore, the ^{17}O echo decay rate dataset obtained for all crystallite orientations in the randomly oriented powders shows that the main fluctuations correspond to Mn magnetic moments aligned along the edges of the cubic unit cell, demonstrating a 1D short-range correlated ordering in the PM phase.

Far above T_N all doped electrons are fast-moving e_g electrons. Their fast motion provides the uniform polarization of the localized spins. As the polarization increases with electron doping, the oxygen-deficient $SrMnO_{3-x}$ is shifted towards the FM metallic state in the PM state.

When approaching T_N the spin density of the doped electrons becomes heterogeneous since some electrons are no more fast moving. We were able to monitor the fraction of fast-moving electrons down to 4 K and show that this fraction becomes negligible in the magnetic ordered phase below 100 K. The other doped electrons slow down their hopping and each of them creates a FM domain. These FM domains were detected below 10 K by probing the Mn nuclei. Indeed, the two well-separated lines of the ^{55}Mn NMR spectra prove the existence of two populations of Mn nuclei, a small fraction forming the FM domains while the majority is in the AF ordered lattice. The FM electron-doped domains can be considered as small-size magnetic polarons (MPs) which significantly contribute to the bulk magnetization of $SrMnO_{3-x}$ at low T.

The low-frequency dynamics of the Mn magnetic moments probed by ^{17}O spin-echo experiments shows a thermal-activated hopping of the MP. The observed trend of the energy barrier of hopping to grow with increasing doping, x, indicates that the de Gennes metallic ground state cannot be achieved in oxygen-deficient $SrMnO_{3-x}$. The random structural defects, i.e., oxygen vacancies destroying the perfectly aligned network of the Mn-O-Mn covalent bonds are probably a major source of adversarial effect on the fast motion of doped electrons at low temperature. Indeed, although their gain in kinetic energy is favored by the orbital degeneracy of the e_g conduction band in the cubic $SrMnO_3$ electron, dynamics slow down.

ACKNOWLEDGMENTS

This work was performed within the state assignment of the Russian Federal Agency of Scientific Organizations (Theme "Spin" No. 01201463330) and supported in part by the grants from the Ural Branch of Russian Academy of Sciences (Project No. 15-9-2-49) and from the Russian Foundation for Basic Research (Project No. 14-02-00203). S.V. and A.G. are grateful to ESPCI for hospitality and support.

[1] M. Hennion, F. Moussa, G. Biotteau, J. Rodriguez-Carvajal, L. Pinsard, and A. Revcolevschi, Phys. Rev. B **61**, 9513 (2000).
[2] H. Terashita and J. J. Neumeier, Phys. Rev. B **71**, 134402 (2005).
[3] J. J. Neumeier and J. L. Cohn, Phys. Rev. B **61**, 14319 (2000).
[4] C. Chiorescu, J. L. Cohn, and J. J. Neumeier, Phys. Rev. B **76**, 020404(R) (2007).
[5] A. Maignan, C. Martin, F. Damay, B. Raveau, and J. Hejtmànek, Phys. Rev. B **58**, 2758 (1998).
[6] E. Granado, N. O. Moreno, H. Martinho, A. Garcìa, J. A. Sanjurjo, I. Torriani, C. Rettori, J. J. Neumeier, and S. B. Oseroff, Phys. Rev. Lett. **86**, 5385 (2001).
[7] A. Trokiner, S. Verkhovskii, A. Yakubovskii, A. Gerashenko, P. Monod, K. Kumagai, K. Mikhalev, A. Buzlukov, Z. Litvinova, O. Gorbenko, A. Kaul, and M. Kartavtzeva, Phys. Rev. B **79**, 214414 (2009).
[8] H. Meskine and S. Satpathy, J. Phys.: Condens. Matter **17**, 1889 (2005).
[9] T. Negas and R. S. Roth, J. Solid State Chem. **1**, 409 (1970).
[10] O. Chmaissem, B. Dabrowski, S. Kolesnik, J. Mais, D. E. Brown, R. Kruk, P. Prior, B. Pyles, and J. D. Jorgensen, Phys. Rev. B **64**, 134412 (2001).

[11] A. A. Belik, Y. Matsushita, Y. Katsuya, M. Tanaka, T. Kolodiazhnyi, M. Isobe, and E. Takayama-Muromachi, Phys. Rev. B **84**, 094438 (2011).
[12] H. Sakai, S. Ishiwata, D. Okuyama, A. Nakao, H. Nakao, Y. Murakami, Y. Taguchi, and Y. Tokura, Phys. Rev. B **82**, 180409 (2010).
[13] J.-S. Zhou and J. B. Goodenough, Phys. Rev. B **68**, 054403 (2003).
[14] L. Vaugier, H. Jiang, and S. Biermann, Phys. Rev. B **86**, 165105 (2012).
[15] D. J. Singh, *Correlated Electrons: From Models to Materials Modeling and Simulation* (Forshungszentrum, Julich, 2012), Vol. 2, p. 463.
[16] P.-G. de Gennes, Phys. Rev. **118**, 141 (1960).
[17] S. Verkhovskii, A. Trokiner, A. Gerashenko, A. Yakubovskii, N. Medvedeva, Z. Litvinova, K. Mikhalev, and A. Buzlukov, Phys. Rev. B **81**, 144415 (2010).
[18] G. Allodi, R. DeRenzi, G. Guidi, F. Licci, and M. W. Pieper, Phys. Rev. B **56**, 6036 (1997).
[19] B. Dabrowski (private communication).
[20] R. E. Watson and A. J. Freeman, *Hyperfine Interactions* (Academic Press, New York, 1967), p. 53.
[21] O. Chmaissem, B. Dabrowski, S. Kolesnik, J. Mais, J. D. Jorgensen, and S. Short, Phys. Rev. B **67**, 094431 (2003).
[22] The magnetization reversal isotherms $M(T \geqslant 40\ \mathrm{K}, H)$ in Fig. 3 show that the magnetic anisotropy field, H_a, which blocks free tilts of the AF domains, does not exceed 0.1 T, and has its value mainly contributed by macroscopic demagnetizing fields of nonspherical-shaped grains of the powders.
[23] A. Narath, *Hyperfine Interactions* (Academic Press, New York, 1967), p. 287.
[24] R. Shulman and S. Sugano, Phys. Rev. **130**, 506 (1963).
[25] J. Owen and J. H. M. Thornley, Rep. Prog. Phys. **29**, 675 (1966).
[26] J. van den Brink and D. Khomskii, Phys. Rev. Lett. **82**, 1016 (1999).
[27] The ratio $J/E_F < 1$ because $S(t_{2g})$ are localized spins in $SrMnO_3$.
[28] J. Briático, B. Alascio, R. Allub, A. Butera, A. Caneiro, M. T. Causa, and M. Tovar, Phys. Rev. B **53**, 14020 (1996).
[29] E. Pavarini and E. Koch, Phys. Rev. Lett. **104**, 086402 (2010).
[30] H. Meskine, H. König, and S. Satpathy, Phys. Rev. B **64**, 094433 (2001).
[31] A. Yakubovskii, A. Trokiner, S. Verkhovskii, A. Gerashenko, and D. Khomskii, Phys. Rev. B **67**, 064414 (2003).
[32] R. Wyckoff, *Crystal Structures: Inorganic Compounds* rx_n,$rnmx_2$,$rnmx_3$ (Wiley & Sons, New York, 1964), Vol. 2, p. 287.
[33] E. Turov and M. Petrov, *Nuclear Magnetic Resonance in Ferro- and Antiferromagnets* (Halsded Press, New York, 1972), p. 206.
[34] The magnetic anisotropy field H_a is expected to be greatly diminished in cubic antiferromagnets; our NMR experiments performed in polycrystalline samples yield a slightly overestimated value of H_a.
[35] T. Takeda and S. Ohara, J. Phys. Soc. Jpn. **37**, 275 (1974).
[36] Contrary to the case of a lightly doped $CaMnO_{3-x}$ [7] for $SrMnO_{3-x}$, our attempts to detect the ^{17}O NMR signal of oxygen with a FM enhanced environment failed, even at low T most probably because the oxygen nuclei spend a too-short time inside the MPs [for instance, we estimated $\tau_1(50\ \mathrm{K}) \sim 6.4 \times 10^{-9}$s for S1].
[37] T. Kohmoto, T. Goto, S. Maegawa, N. Fujiwara, Y. Fukuda, M. Kunitomo, and M. Mekata, Phys. Rev. B **49**, 6028 (1994).
[38] S. H. Baek, F. Borsa, Y. Furukawa, Y. Hatanaka, S. Kawakami, K. Kumagai, B. J. Suh, and A. Cornia, Phys. Rev. B **71**, 214436 (2005).
[39] R. Walstedt, Phys. Rev. Lett. **19**, 146 (1967).
[40] C. P. Slichter, *Principles of Magnetic Resonance* (Springer-Verlag, Berlin, 1990), p. 640.
[41] A. Trokiner (private communication).
[42] A. M. Oleś and G. Khaliullin, Phys. Rev. B **84**, 214414 (2011).